Model-Based Analysis of Arabidopsis Leaf Epidermal Cells Reveals Distinct Division and Expansion Patterns for Pavement and Guard Cells[1][W][OA]

Leila Kheibarshekan Asl[2], Stijn Dhondt[2], Véronique Boudolf, Gerrit T.S. Beemster, Tom Beeckman, Dirk Inzé, Willy Govaerts, and Lieven De Veylder*

Department of Applied Mathematics and Computer Science, Ghent University, 9000 Ghent, Belgium (L.K.A., W.G.); Department of Plant Systems Biology, VIB, 9052 Ghent, Belgium (L.K.A., S.D., V.B., G.T.S.B., T.B., D.I., L.D.V.); Department of Plant Biotechnology and Bioinformatics, Ghent University, 9052 Ghent, Belgium (S.D., V.B., G.T.S.B., T.B., D.I., L.D.V.); and Department of Biology, University of Antwerp, 2020 Antwerp, Belgium (G.T.S.B.)

To efficiently capture sunlight for photosynthesis, leaves typically develop into a flat and thin structure. This development is driven by cell division and expansion, but the individual contribution of these processes is currently unknown, mainly because of the experimental difficulties to disentangle them in a developing organ, due to their tight interconnection. To circumvent this problem, we built a mathematic model that describes the possible division patterns and expansion rates for individual epidermal cells. This model was used to fit experimental data on cell numbers and sizes obtained over time intervals of 1 d throughout the development of the first leaf pair of Arabidopsis (Arabidopsis thaliana). The parameters were obtained by a derivative-free optimization method that minimizes the differences between the predicted and experimentally observed cell size distributions. The model allowed us to calculate probabilities for a cell to divide into guard or pavement cells, the maximum size at which it can divide, and its average cell division and expansion rates at each point during the leaf developmental process. Surprisingly, average cell cycle duration remained constant throughout leaf development, whereas no evidence for a maximum cell size threshold for cell division of pavement cells was found. Furthermore, the model predicted that neighboring cells of different sizes within the epidermis expand at distinctly different relative rates, which could be verified by direct observations. We conclude that cell division seems to occur independently from the status of cell expansion, whereas the cell cycle might act as a timer rather than as a size-regulated machinery.

In most plant species, the above-ground plant body is dominated by leaves, the organs specialized in photosynthesis. This process converts carbon dioxide into organic components utilizing energy from sunlight, making leaves the energy production site and the growth engine of plants. To maximize its light-capturing capacity, a leaf is typically flat and thin. This characteristic shape is established during the leaf developmental process. Leaves arise on the flanks of the shoot apical meristem (SAM) at auxin accumulation sites (Benková et al., 2003). At these positions, a number of cells start to bulge out from the meristem and eventually will form the basis of the leaf primordium when cell division proceeds (Reinhardt et al., 2000; Pien et al., 2001). Dorsiventrality is specified early during primordium development and defines the adaxial and abaxial sides of the leaf (Bowman, 2000). Divisions at the margin of the primordium drive leaf blade inception. Further expansion of the leaf blade is controlled by a strong preference for anticlinal divisions, leading primarily to lateral outgrowth of the different tissue layers, of which the epidermis is the main layer driving leaf growth (Donnelly et al., 1999; Savaldi-Goldstein et al., 2007).

During leaf development of dicotyledonous species, a cell proliferation phase, characterized by actively dividing cells, is followed by a cell expansion phase, characterized by cell growth and differentiation. After expansion, cells mature and the final leaf size is reached (Beemster et al., 2005). At the proliferation-to-expansion phase transition, cell division ceases along a longitudinal gradient from leaf tip to base (Donnelly et al., 1999). In the epidermis, the onset of differentiation coincides with the formation of stomata (De Veylder et al., 2001). A stomatal complex consists of two guard cells that control the aperture of the stomatal pore. Starting from a precursor meristemoid cell, a series of subsequent asymmetric divisions produce a

number of guard mother and daughter cells. Subsequently, the guard mother cells divide symmetrically into two guard cells, ending the stomatal lineage. The daughter cells undergo cell fate specifications identical to those of the majority of the cells produced during the proliferation phase, resulting in puzzle-shaped pavement cells (Larkin et al., 1997; Geisler et al., 2000).

The final leaf size is determined by the total number of cells and the average cell size that result from cell division and cell expansion, respectively. Although the dynamics of these processes can be analyzed rigorously by the leaf growth kinematics (Fiorani and Beemster, 2006), knowledge of cell cycle duration, cell expansion, and their interaction at the individual cell level is still poorly understood, not only because of technical obstacles to study these phenomena, but also because a reduced cell proliferation is often compensated by an increase in cell size and vice versa (Tsukaya, 2002). Here, the individual cell sizes of pavement and guard cells were measured separately throughout leaf development. By fitting a mathematical model to these data, we could estimate the division and expansion parameters of pavement and guard cell populations within the growing leaf separately, allowing us to gain a better and more detailed insight into the processes that define leaf growth. Imaging of epidermal cells gave a good correlation between predicted and experimental cell growth data, supporting the model.

RESULTS

### Following Leaf Growth during Development

Recent developments in microscopic and imaging technologies suggest that cell tracking is the most suitable manner to disentangle cell division and expansion in plants, allowing cells to be followed for 3 to 4 d and applied successfully to the root, the SAM, and sepals (Reddy et al., 2004; Campilho et al., 2006; Fernandez et al., 2010; Roeder et al., 2010). However, to cover the entire leaf development, a much longer time frame is needed. Furthermore, with these techniques only local observations can be made, which are not always easily correlated to global growth characteristics. Therefore, a general kinematic analysis of leaf growth in Arabidopsis (*Arabidopsis thaliana*) was used as a starting point (De Veylder et al., 2001). In this approach, the first developing leaf pair (leaves 1 and 2) was harvested on a daily basis 5 to 25 d after sowing (DAS). Leaves 1 and 2 were selected because they are nearly indistinguishable and probably the best synchronized among replicate plants. Microscopic drawings of abaxial epidermal cells were made at 25% and 75% of the distance from the base to the tip of the leaf, giving an estimate of the average cell area. To approximate the total cell number per leaf, these average cell areas were combined with the measured total leaf area. When analyzed on a daily basis, average cell division

and relative expansion rates can be calculated. Plotting of the leaf size evolution on a logarithmic scale revealed a linear increase until day 11, indicating exponential growth (Fig. 1A). From day 12 onward, relative leaf expansion rates decreased and the mature leaf size was reached approximately at 20 DAS. A similar evolution could be observed for the total cell number (Fig. 1B), with cell division rates being high until day 10 (Fig. 1C). Cell sizes remained relatively constant until day 10 (approximately 100 μm^2), whereas from day 10 onward, the average cell size increased approximately 10-fold by day 20, as the result of cell expansion in the absence of cell division (Fig. 1D). Coinciding with the decrease in cell division rate, the stomatal index (fraction of guard cells among all cells) increased linearly (Fig. 1E). The relative leaf expansion rates were the highest during the high division rate period (Fig. 1F). When pavement and stomatal cells are considered separately, the total number of pavement cells increased gradually from day 5 to 14, while the number of guard cells continued to increase until day 17 (Supplemental Fig. S1), indicating that divisions giving rise to guard cells continued approximately 3 d longer than those forming pavement cells.

Cell Size Distributions

Although the kinematic data give an indication of the general growth processes during leaf development, leaves are considered as homogenous cell populations, which is a simplification because the epidermis consists of multiple cell types, each with distinct size characteristics at different time points during development. Furthermore, pavement cells and guard cells are interdependent, because pavement cells are formed together with stomata (Geisler et al., 2000). Additionally, the size of pavement cells ranges from 50 up to 20,000 μm^2, illustrating the heterogeneity of the population. A better insight into the cell area distribution was gained by extension of the image analysis algorithm used for the kinematic analysis to allow size measurements of individual guard and pavement cells. To ascertain that the obtained data were representative for the complete leaf, we compared the data obtained from extrapolation of the measurements of cell sizes at two reference positions (25% and 75% between base and tip of the leaf blade) with those of microscopic drawings of five complete leaves at the transition from cell proliferation to cell expansion (namely in 9-d-old leaves). At this time point, the largest differences across the leaf would be expected because of the cell cycle arrest front that propagates along the leaf axis (Donnelly et al., 1999). Comparison of the data extracted from the complete leaves with those from the leaf reference sections revealed no significant differences for the average cell number and cell area. Furthermore, plotting of the cell size distributions also yielded a good overlay between the data resulting from the complete leaf and the leaf sections (Supplemental Fig. S2), demonstrating that the data

Figure 1. Kinematic growth data for the first true leaf pair of Arabidopsis seedlings. A, Leaf area. B, Total cell number. C, Cell division rate. D, Mean cell area. E, Stomatal index. F, Relative leaf elongation rate.
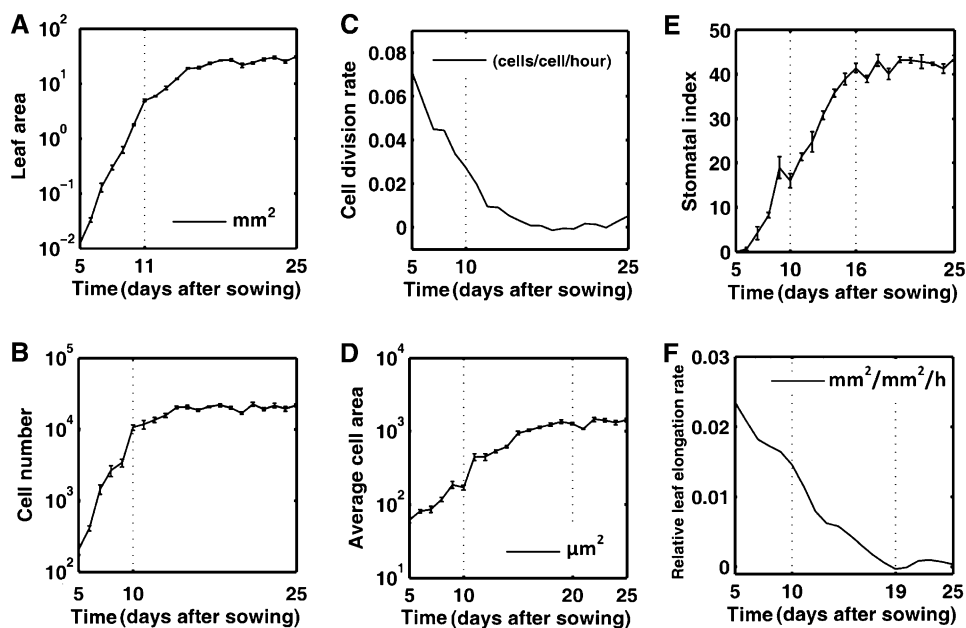
sampling at the two reference positions is a valid approach to estimate cellular parameters for the complete leaf.

According to the cell area measurements as described above, 97% of the pavement cells of 5-d-old leaves were smaller than 100 μm^2, whereas at day 8, only 62% of the cells had a size below this threshold, indicating that pavement cell sizes increase already during the cell proliferation phase. Early in the expansion phase, at 10 DAS, the maximum cell size detected was approximately 1,600 μm^2 and 95% of the pavement cells were smaller than 500 μm^2. From day 11 onward, the pavement cell area distribution broadened and the pavement cell population was distributed over a large range of cell sizes (Fig. 2A). Guard cell sizes ranged from 25 to 150 μm^2, with a mean area of approximately 75 μm^2. During leaf development, cell sizes increased continuously, reaching a maximum size of approximately 300 μm^2 and an average area of 150 μm^2 at 25 DAS (Fig. 2B).

To obtain quantitative information about the changes in cell size distributions during leaf development, we used the frequency distribution of the cell areas of pavement and guard cells for the whole leaf on day i (for details, see Supplemental Text S1). This absolute representation of the data revealed that from day 5 to 12, most pavement cells were very small (less than 300 μm^2) and that the number of these small cells increased significantly from day 6 to day 9 (Fig. 2C), corresponding to the high cell division rate during these days. From day 9 until day 12, the peak of the distribution curves was less pronounced and was accompanied by a high proportion of large cells, of which the number increased until day 17, after which the distribution of pavement cells remained relatively stable. The guard cell distribution was different. The

graph had a symmetrical bell shape with a peak at the mean, revealing a roughly normal size distribution of guard cell sizes (Fig. 2D). Prior to day 9, the number of guard cells was low, but afterward increased significantly until day 17, indicating that most divisions of guard mother cells, leading to the formation of stomata, occurred relatively late during the epidermal development. After day 17, the complete guard cell size distribution continued to shift to the right, implying that cells had ceased dividing and continued to expand.

Mathematical Model for Leaf Development

To study in more detail the crucial parameters for cell division and cell expansion during leaf development, we built a general mathematical model that takes only the pavement and guard cells into account, because in our experimental system it is impossible to distinguish pavement from stomatal precursor cells. The model is based on the overall kinematics of leaf growth (Fig. 1), on the changes in size distribution of pavement and guard cells between successive days in function of cell expansion (Fig. 2), and on the changes in cell identity with each division event. Therefore, all possible transitions were considered that a cell can undergo from one day to the next: A precursor cell might either expand and divide into two pavement cells or two guard cells, or expand in the absence of division, whereas guard cells do not divide, but can expand. The model included a maximum guard cell size (GC_{max}). As the final division in the stomatal lineage is symmetric, pavement cells larger than twice this size ($2GC_{max}$), cannot divide into two guard cells. Additionally, a hypothetical threshold was introduced above which pavement cells can no longer divide
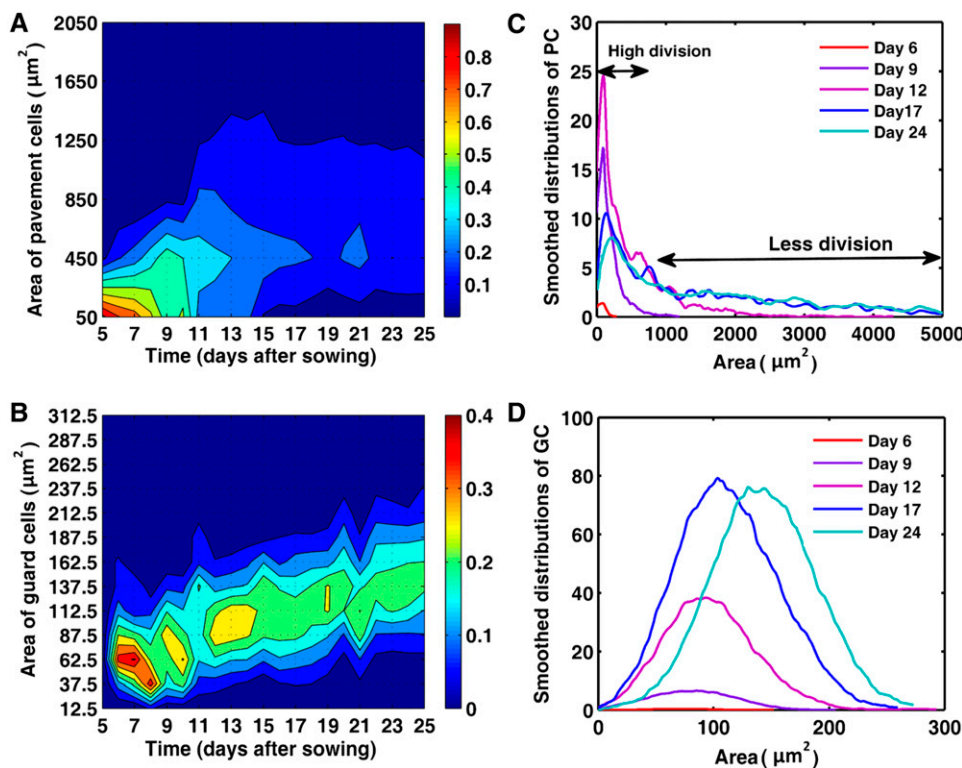
Figure 2. Cell size distributions during leaf development. A and B, Size distribution of pavement (A) and guard (B) cells in the abaxial epidermis of leaves 1 and 2. Color ranges indicate the fraction of the total number of cells present within a specific size bin. The vertical axis shows bins of cell areas (bin size is 400 μm^2 and 25 μm^2 for pavement and guard cells, respectively). Labels on the vertical axis mark the beginning of each bin. Red and blue correspond to high and low percentage of cells, respectively. The colors in the ranges between two consecutive bins are obtained by interpolation. C and D, Distribution of the number of pavement (C) and guard (D) cells per leaf during its development.

(PC_{max}). Apart from these, specific parameters used in the model were the average cell cycle duration time (T_c), average relative cell growth rates for pavement (g_{PC}) and guard cells (g_{GC}), and the probabilities p_1 and p_2 for a precursor cell to divide into pavement or guard cells, respectively. p_3 (equal to $1 - p_1 - p_2$) represented the probability for a pavement cell not to divide during a 24-h period. These probabilities represent different developmental pathways at the population level, rather than the status of an individual cell. This means that in principle cells that did not divide at day i, and in this way contribute to p_3 at that day, can still divide at day $i + 1$. This restriction to the population level is intrinsic to kinematic growth analysis, which does not track individual cells. PC_{max}, T_c, g_{PC}, g_{GC}, p_1, and p_2 are allowed to vary from day to day, whereas GC_{max}, as a maximum size, remains constant throughout development.

Subsequently, we identified the different developmental categories for pavement cells at any given day (Fig. 3A). The first category contains cells with an area below $2GC_{max}$ that can either divide into pavement or guard cells or stop dividing, contributing to fractions p_1 and p_2. The second category contains cells with an area between $2GC_{max}$ and PC_{max} that can no longer become guard cells, because the resulting cells would exceed the maximum threshold size for guard cells. Therefore, a fraction p_1 of the cells in this category divided into pavement cells and the remainder ($1 - p_1$) expanded without division. The third category contains cells with an area above PC_{max} that can no longer divide.

A precursor cell with an area a^* at day i could develop into a cell with area a at day $i + 1$ through several scenarios, called flows. These flows were defined by the state of cells at day i and $i + 1$ and the number of divisions required for the corresponding transition. Due to the 1-d time steps in the experimental data, in particular whether T_c is <24 h or ≥24 h, strongly affects the possible number of divisions during this time interval. The average cell cycle duration in a fully proliferating tissue, represented by days 5 to 8 in our analysis, was calculated to be 25.6 ± 5.4 h (Supplemental Table S1). In a previous study, the average cell cycle duration for a fully proliferating tissue was found to be 20.7 h (De Veylder et al., 2001). Thus, to simplify the model, we restricted the parameter space by assuming that (on average) T_c ≥ 18 h, implying that each pavement cell can undergo at most two divisions in 1 d.

Based on these assumptions, eight possible flows (F_1–F_8) for pavement cells and one flow (F_9) related to guard cells were defined (Fig. 3B). Flow F_1 involves pavement cells that do not divide in 1 d, but only expanded. For dividing cells, possibilities differ based on whether the cell cycle duration time is shorter or longer than 24 h. For flows F_2, F_3, and F_6, T_c was ≤24 h and pavement cells divide within 1 d either once (F_2) or twice (F_3) into pavement cells or guard cells (F_6). In flow F_3, for the sake of simplicity, both newborn pavement cells are assumed to be dividing into pavement cells. Because T_c > 18 h, not many cells take part in this flow and therefore the number of missed events

Figure 3. Different scenarios of division and expansion of pavement and guard cells over a 1-d interval. A, Size categories of pavement cells. B, Global scheme of the possible flows for pavement and guard cells. The flows are defined based on the fates of the cells and the duration of the cell cycle. PC and GC, Pavement and guard cells, respectively.
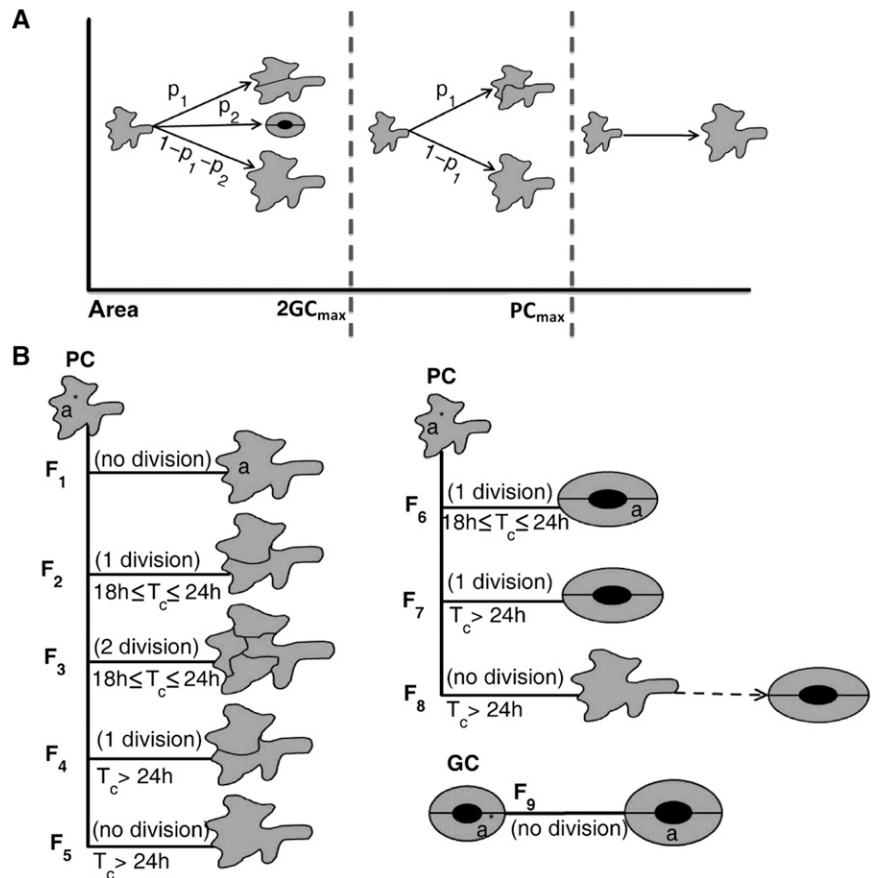
must be small. When $T_c > 24$ h, pavement cells can divide at most once in 1 d. In flow F_4, pavement cells divide once, while in flow F_5, they were dividing, but do not complete their division cycle within the 1-d time step. Flow F_7 is related to the pavement cells that divide into guard cells and flow F_8 to those that are in the process of dividing into guard cells, but do not complete the division in the 1-d time step. Finally, flow F_9 represents guard cells that expanded only.

For these flows, we constructed functions for the transitions between the size distributions of pavement and guard cells from a given day i, to the next. Although all flows differed, they have a common basic structure. To describe these functions mathematically, we introduced $G_k^i(a^*)$ as the distribution of cells (pavement or guard cells) with area a^* at day i that are transformed by the k-th flow and $F_k^{i+1}(a)$ as the distribution of cells (pavement or guard cells) with area a at day $i + 1$ into which they are transformed. We also introduced $f_{2,k}$ as a function defined by $f_{2,k}(a) = a^*$, meaning that a cell with area a at day $i + 1$ originates from a cell with area a^* that follows the k-th flow at day i. Therefore, for a small distance ε, the radius around a is:

$$f_{2,k}(a - \varepsilon) = a^* - \varepsilon_1 \tag{1}$$

$$f_{2,k}(a + \varepsilon) = a^* + \varepsilon_2 \tag{2}$$

where ε_1 and ε_2 are both approximately equal to $\frac{df_{2,k}(a)}{da}\varepsilon$. If $N_k(\varepsilon)$ is the number of cells at day $i + 1$ in $[a - \varepsilon, a + \varepsilon]$ that originates from the k-th flow, then this corresponds to $\frac{N_k(\varepsilon)}{n_k}$ cells in $[a^* - \varepsilon_1, a^* + \varepsilon_1]$ at day i, where n_k is the number of cells at day $i + 1$ that originate from one cell at day i through the k-th flow. Hence, the distribution of cells with area a at day $i + 1$ is given by:

$$F_k^{i+1}(a) = \lim_{\varepsilon \to 0} \frac{N_k(\varepsilon)}{2\varepsilon} = \lim_{\varepsilon \to 0} \frac{\frac{N_k(\varepsilon)}{n_k}}{\varepsilon_1 + \varepsilon_2} n_k \lim_{\varepsilon \to 0} \frac{\varepsilon_1 + \varepsilon_2}{2\varepsilon} \tag{3}$$

$$= G_k^i(a^*) n_k \lim_{\varepsilon \to 0} \frac{\varepsilon_1 + \varepsilon_2}{2\varepsilon} \tag{4}$$

$$= G_k^i(f_{2,k}(a)) f_{1,k}(a) \tag{5}$$

where $f_{1,k}(a) = n_k \frac{df_{2,k}(a)}{da}$. The mathematical description of each flow and explicit form of each $f_{1,k}$ and $f_{2,k}$ is given in the model file (see Supplemental Text S1). Using the functions $F_1, F_2, \ldots F_9$, we predicted the distribution of cells with area a at day $i + 1$ as follows

$$D_{PC}^{i+1}(a) = \sum_{k=1}^{5} F_k^{i+1}(a) + F_8^{i+1}(a) \tag{6}$$

$$D_{GC}^{i+1}(a) = \sum_{k=6}^{7} F_k^{i+1}(a) + F_9^{i+1}(a) \qquad (7)$$

where $D_{PC}^{i+1}(a)$ and $D_{GC}^{i+1}(a)$ are the predicted distributions of pavement and guard cells, at day $i + 1$, respectively. The right-hand sides of Equations 6 and 7 are obtained by using Equation 5 and the experimental distributions of pavement and guard cells at day i.

Parameter Estimation

The predicted distributions (Eqs. 6 and 7) were used to optimize the value of the parameters on which the functions F_1, F_2,...F_9 depend, by optimizing the fit to the experimental data. To assess the optimization problem, two phases in the development of the leaf are considered: one that represents days 5 to 17, when cells divide regularly, implying that both cell division and expansion might happen simultaneously for some cells, and one from days 18 to 25, when the final cell numbers are reached and all cells stop dividing (Supplemental Fig. S1). Absence of cell division in the second stage of development reduces the number of parameters because both probabilities p_1 and p_2 are 0. Moreover, because of the lack of cell division, the maximum threshold for cell division of pavement cells (PC_{max}) is irrelevant and can be eliminated. Therefore, g_{PC}, g_{GC}, and GC_{max} are the remaining parameters to be estimated within the second phase of development.

In the first phase of development, some a priori restrictions to the model are imposed to reduce the range in which parameters needed to be optimized. First, because no cell can divide into guard cell and pavement cell simultaneously, it is considered that $p_1 + p_2 \leq 1$. Second, we assume that at the early stages of leaf development all cells divide ($p_1 + p_2 = 1$ at days 5, 6, and 7), which is supported by the uniform expression of cell cycle marker genes in young leaves (de Almeida Engler et al., 2009). Accordingly, the number of cells during early leaf development approximately doubled every 24 h (Supplemental Table S1). Lastly, based on the size increase of guard cells over time (Fig. 2B), the maximum threshold for precursor cells to divide into guard cells ($2GC_{max}$) is based on GC_{max} computed in the second phase, which is then applied to the first phase. With the model and the experimental distributions of the pavement and guard cells on a given day, we predicted the distributions for the next day. Although a best fit for the distribution of the guard cells at the earliest time points was difficult to find because of the low number of guard cells at the early stage of leaf development, experimental and computed data fitted well from 9 DAS onward (Supplemental Figs. S3 and S4).

Constancy of Average Cell Cycle Duration

Cell division rates quantify the rate at which cells progress through the cell cycle. In the kinematic growth analyses, the cell division rate decreased progressively

(Fig. 1C). However, because division rates are calculated based on the total number of leaf cells, the observed decrease might be due to a reduction in the fraction of cells proliferating, an increase in the average cell cycle length, or a combination of both. To understand how the average division rate is controlled, it is essential to quantify the fraction of cells dividing into pavement (p_1) and guard (p_2) cells. As computed by the model, p_1 decreased gradually during leaf development, while p_2 increased, indicating a shift from basal proliferation to cell division in the stomatal lineage (Fig. 4A). The probability p_2 had the largest values between days 10 to 14, meaning that most stomata were produced during these days. After day 14, both probabilities dropped and decreased to 0, representing the exit of cell division during leaf development as indicated by an increase in probability p_3, in which more than 80% of the cells did not divide after day 16.

Because the model allows us to split the total number of cells in a proliferative and an expanding population at the different stages of leaf development, a slow down in the cell division rate can be discriminated from a reduction in the proliferative fraction.
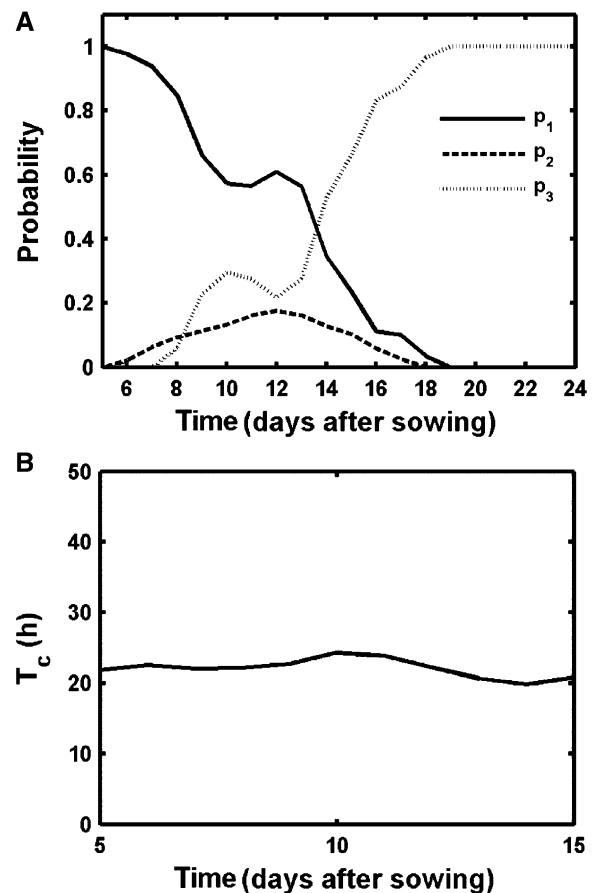

Figure 4. Predicted cell division parameters during leaf development. A, Probabilities for alternative divisions; p1: pavement cells, p2: guard cells, p3: no division. B, Average cell cycle duration.

Average cell cycle duration (T_c) can be derived from the cell division rate and was determined for each day during leaf development. As discussed above, the impact of T_c in the model ended after day 18, when cell division stopped completely. Immediately prior to that, between days 16 and 18, the optimization results fluctuated a lot (Supplemental Fig. S5), implying that the proliferative fraction was too small to obtain reliable results. For earlier time points, however, a stable output value was obtained. Remarkably, when different days are compared, the obtained T_c value is nearly constant (Fig. 4B), indicating that the reduced cell division rate over the complete leaf during development by kinematic analysis was seemingly not caused by an increase in average cell cycle duration, but solely by a decrease in the proliferative fraction within the leaf.

Nonexistence of Size Threshold for Division

One of the parameters included in the model was the maximum guard cell size GC_{max}, which was designated a maximum threshold because guard mother cells, identified as pavement cells in our analysis, must have an area smaller than $2GC_{max}$ as a necessary condition for division into guard cells. As discussed above, the threshold for guard cells was calculated easily in the second stage of development (from days 18–25), when no cells divided. When we assumed the threshold to be constant, the parameter optimization procedure provided a value equal to 354 μm^2, which was only a little above that of the maximum guard cell size

of 300 μm^2 found in the experimental data (Fig. 2), illustrating the accuracy of the optimization methods. The value of GC_{max} indicated that cells with an area larger than approximately 700 μm^2 are unable to divide into guard cells.

In contrast to the robust value obtained for GC_{max} in nearly all simulations, the optimized parameter value for the threshold above which no divisions into pavement cells occur (PC_{max}) yielded erratic values. In cases with an optimal solution, the experimental cell size distribution (used to build the model) and the computed cell size distribution profiles strongly deviated (Fig. 5, A and B), implying that the found optimum was a spurious one. To strengthen this observation, simulations were done with fixed values for PC_{max} = 300, 500, 1,000, and 10,000 μm^2 at day 11 to 12, when the leaf consists of both dividing and expanding cells. Consistently with the behavior of the model with fitted PC_{max}, small fixed values of PC_{max} resulted in a sharp deviation from the experimental data (Fig. 5C). As the PC_{max} value increased, the discrepancy between experimental and computed data gradually disappeared, which might be explained by the fact that most cells were smaller than the threshold and, thus that the PC_{max} value became less relevant. These observations demonstrate that the imposition of a threshold value for cell division in pavement cells is not compatible with the assumptions underlying the model. The nonexistence of a threshold for pavement cell division indicates that the size of a cell does not exclude it from dividing into a set of pavement cells, i.e. size alone does not prevent division. In accordance with this

Figure 5. Observed and predicted pavement cell size distribution with optimized and imposed PC_{max} values. A and B, Comparison between the experimental and predicted pavement cell size distribution with optimized PC_{max} for day 12 (A) and day 14 (B). C, Comparison for different imposed values of PC_{max} at day 12. PC, Pavement cells.
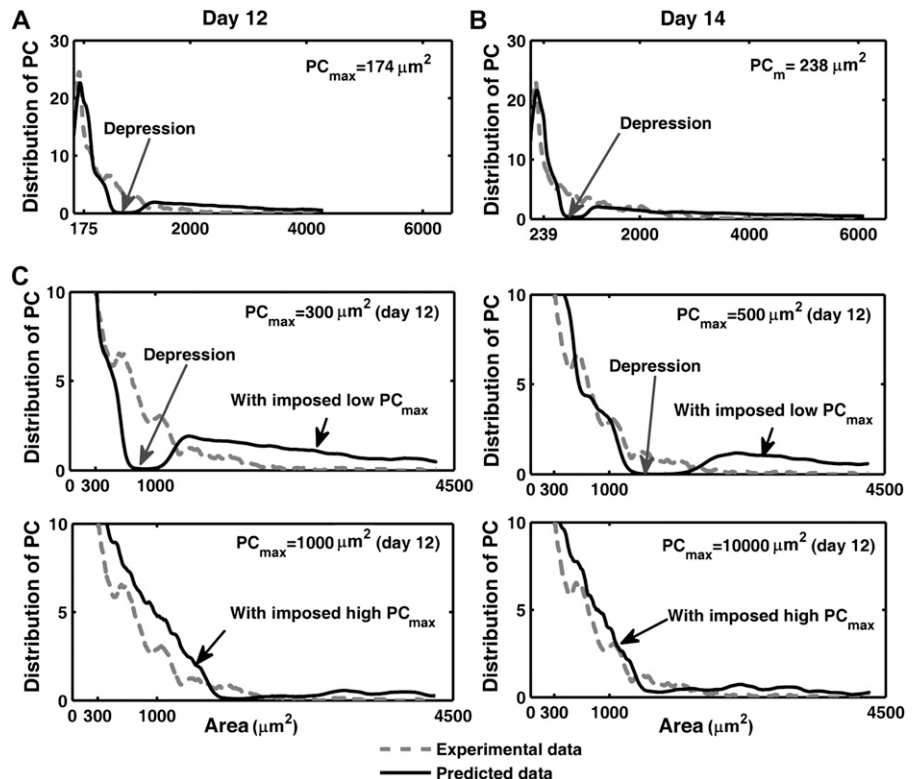
model prediction, pairs of relatively large pavement cells separated by a straight cell wall, indicative of a recent cell division event, could be observed in the epidermis of 14-d-old leaves (Supplemental Fig. S6).

Growth Rates of Epidermal Cells

The difference in maximum cell sizes found for pavement and guard cells suggests that the two cell types might expand at different rates. Therefore, the model allows for different relative growth rates (RGRs) for pavement and guard cells. Cell division and cell expansion are considered independently and RGRs do not only apply to expanding, but also proliferation cells.

The model results indicated that pavement cells had a high and increasing RGR from day 5 to day 13, with a profound increase between day 10 and 13 (Fig. 6A). From day 13 onward, the RGR declined steeply, suggesting that pavement cells grew faster in the young proliferating than in the older expanding leaves. Eventually, growth stopped completely after day 18. These observations are consistent with the experimental data because the average cell area of pavement cells increased from 86 μm^2 in the young leaf to nearly 1,500 μm^2 between days 7 and 16, but did not change

significantly after that (Fig. 1D). Similarly, guard cells displayed higher RGRs in the young than in the old leaves. Initially, the RGR of pavement cells was higher than that of guard cells, but from day 18 onward, stomata grew faster than pavement cells (Fig. 6A).

After day 18, pavement cells did not divide; hence, the RGR of small pavement cells ($<300\ \mu m^2$) could be calculated by measuring the shift in the distribution peak in the experimental size distribution graphs (Fig. 2C). The average RGR of small cells determined this way was 0.009/h, whereas the average RGR from day 18 until day 25 for all pavement cells calculated by the model was 0.0009/h (Fig. 6A). These results suggest that during the last days of leaf development, small pavement cells grow 10-fold faster than the average population. To confirm the surprising finding that adjacent cells of different size grow at different rates, we performed confocal imaging to directly measure RGRs for individual pavement and guard cells over a 36-h time interval. Cell-tracking experiments on leaves at 17 DAS confirmed that pavement cells smaller than 300 μm^2 grew faster than large ones (P value = 3.65e-5, Student's t test; Fig. 6, C and D). The average RGRs of small pavement cells decreased steeply from approximately 0.015 to 0.005 in the size range between 30 and 300 μm^2. In larger cells, a relatively constant RGR was
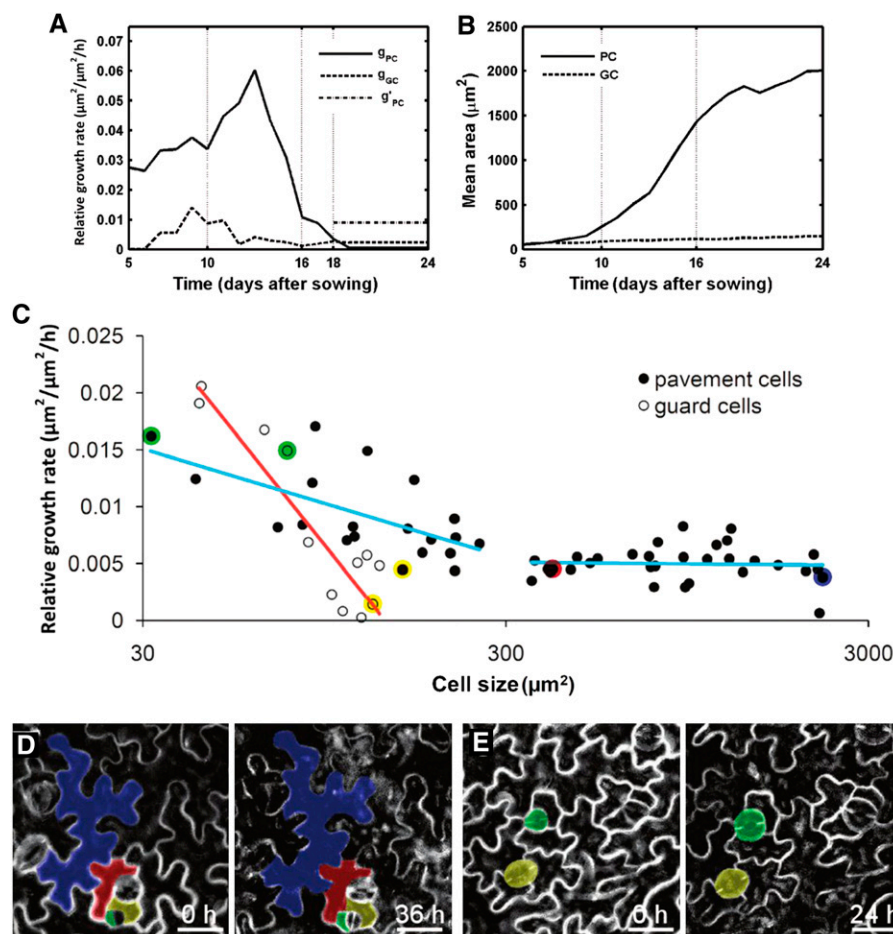

Figure 6. Differential cell growth rates during leaf development. A, Average RGRs of pavement (g_{PC}) and guard cells (g_{GC}). g'_{PC} is the experimentally observed average RGR of small pavement cells from days 18 to 25. B, Experimental mean area of pavement and guard cells. C to E, Live imaging of epidermal cell growth in leaves. C, RGRs of pavement and guard cells on the abaxial epidermis of leaves 1 and 2 of 17-d-old plants over a period of 36 h. Red and blue lines indicate a logistic regression for guard and pavement cells, respectively. Colored dots represent data of individual pavement and guard cells depicted in sections D and E. D, Time-lapse observations of epidermal cell development over a 36-h interval. E, Time-lapse observation of guard cells over a 24-h interval. Scale bars = 25 μm.

measured. Small guard cells ($<100\ \mu m^2$) also grew faster than large ones (P value = 0.0017, Student's t test; Fig. 6, C and E). In contrast to pavement cells, guard cells did not display a biphasic growth pattern, but a steady decrease in RGR with their cell size. Strikingly, at the transition of day 17 to 18 the average RGR of pavement cells measured by live imaging (0.0065/h) was nearly identical to the value obtained by the model (0.0061/h), independently confirming the model predictions (Fig. 6A).

DISCUSSION

Leaf development of Arabidopsis is driven by two processes, cell division and cell expansion (Green and Bauer, 1977). As both processes are intimately intertwined, their individual contribution to leaf growth is not easily studied experimentally. Here, we developed a mathematical model based on the fates of the two epidermal cells types found in the abaxial epidermis of the first leaf pair of Arabidopsis to fit experimentally derived data obtained over the course of its development from a young dividing leaf primordium into an adult organ. This model allowed us to disentangle cell division and cell expansion parameters for the individual cell types.

Differential Cell Expansion within the Leaf Epidermis

Individual cell size measurements yielded cell area distributions during leaf development. When the RGRs of guard cells and pavement cells were compared, the growth of these two cell types followed distinctly different dynamics. The guard cells initially grow more slowly but steadily, whereas the large pavement cells initially grow faster, but stop around day 16. Differences in RGRs between adjacent cells are surprising and have, to our knowledge, not been investigated in leaves. In the root, this problem has been studied by measuring cell sizes of different cell types (Beemster and Baskin, 1998). Root growth is linear and symplastic, meaning that neighboring cells grow uniformly, without altering the positions of adjacent walls. As a consequence, at a given distance from the tip, all cells have by definition the same relative elongation rate (Green, 1976). This constraint implies that differences in mature cell sizes reflect differences in cell proliferation (Beemster and Baskin, 1998). In comparison, leaf growth is much more complex. As a leaf is a flat, exponentially growing structure with small and large cells dispersed over the epidermal surface, several parameters have to be taken into account in the equations. Time-lapse cell-tracking experiments on 17-d-old leaves indicate that small pavement and guard cells grow faster than large cells. Furthermore, modeling results indicated that relative cell growth rate of pavement cells is tightly regulated during development, peaking during the early leaf expansion phase, followed by a rapid reduction and no growth

occurring at maturity. In other words, cells exiting the proliferative status grow faster than those being in full expansion phase. A high increase in the RGR was seen between days 10 and 14. Interestingly, this time frame coincides with the strongest increase in cellular DNA content through endoreduplication (Supplemental Fig. S7). During the endoreduplication cycle, cells do not divide but continue to increase their DNA content. A positive correlation is often seen between cell size and the level of endoreduplication (Sugimoto-Shirasu and Roberts, 2003). The observed correlation between the increase in relative cell growth rate and elevation in DNA content supports the generally assumed hypothesis that endoreduplication drives cell growth.

Taken together, the model reveals substantial differences in RGRs within the epidermal layer. Because guard cells, and small and large pavement cells are dispersed throughout the leaf, due to the patterning in the stomatal lineage, adjacent guard and pavement cells of various sizes might expand at different relative rates within the developing epidermis. Differential expansion of tissue layers in cylindrical organs, such as stems and roots, results in tissue tension, often redirecting growth, as in the case of shoot phototropism and root gravitropic curvature (Liscum and Stowe-Evans, 2000; Swarup et al., 2005). Leaf epinasty is also the consequence of differential growth of the abaxial and adaxial sides (Keller and Van Volkenburgh, 1997). Within one single tissue layer of a flat tissue structure, such as the abaxial leaf epidermis, tension is more difficult to translate into motion to release pressure. Disturbance of symplastic growth in the root by inducing differences in relative cell expansion rates between tissue layers causes cells to rupture and distort root growth (Ubeda-Tomás et al., 2009). However in the leaf, no cell ruptures are detected within the epidermis. Possibly, the lobes of epidermal pavement cells offer a way to dissipate the tissue tension. Remarkably, the characteristic jigsaw puzzle shape of pavement cells is established at the proliferation-to-expansion transition. Thus, the appearance of the puzzle shape fits with the moment at which differential relative cell expansion rates in adjacent cells would first appear. Furthermore, the emergence of lobes leading to the puzzle shape is preceded by the reorganization of cortical microtubules (Panteris and Galatis, 2005; Kotzer and Wasteneys, 2006) and application of external mechanical stresses to a tissue results in realignment of microtubules parallel to the maximal stress directions (Hamant et al., 2008). Based on these observations, it could be speculated that the occurrence of tissue tension within the epidermis layer, caused by differential cell expansion, might realign cortical microtubules and trigger the puzzle-shape formation. More experimentation will be required to validate this intriguing hypothesis.

Interestingly, at maturity, the guard cells in Arabidopsis leaves are elevated above the surrounding pavement cells, presumably to increase their evaporative capacity. Faster relative growth of the guard cells and

surrounding smaller pavement cells compared to the larger pavement cells that make up the bulk of the tissue area could explain the development of this elevation.

Control of Cell Cycle Duration

In the root, divisions in the meristematic zone ensure a constant cell production and indeterminate growth. While cells mature, they are displaced from the root tip and enter the elongation zone (Beemster et al., 2003). Thus, in the root, the developmental stages are separated in space. Furthermore, in the root meristem, practically all cells divide actively, implying that the cell division rate calculated for the meristem is a good overall average. In contrast, in leaves, the developmental stages are separated in time. Moreover, at the proliferation-to-expansion phase transition, the cell cycle arrest front that follows a longitudinal gradient, is accompanied by the differentiation of the first stomata (Donnelly et al., 1999; De Veylder et al., 2001), whereas cells at earlier stages in the stomatal lineage, dispersed through the leaf, keep proliferating for multiple days (Bergmann and Sack, 2007). Because of these constraints, the average cell division rate calculated on the basis of an increase in total cell number can only be measured experimentally during the early developmental stages, when all cells participate in division. Our mathematical model yielded probabilities for a cell to divide into two pavement cells, into two guard cells, or to exit the mitotic cycle, allowing the calculation of the proliferative fraction and the corresponding average cell cycle duration throughout the complete leaf development. Surprisingly, although the cell cycle length can vary significantly between adjacent cells within the SAM and sepals (Reddy et al., 2004; Roeder et al., 2010), the average cell cycle duration over the complete leaf epidermis remained constant during development. This observation is analogous to the situation in roots, where average cell cycle duration is considered to be constant between cell types and between different positions in the meristem (Ivanov et al., 2002). Moreover, the average cell cycle duration of approximately 20 h found for the leaf is comparable to that for the root (Beemster and Baskin, 1998). These data indicate that the constancy of cell cycle duration is widespread and that the basal cell division rate is strongly conserved at a cellular level (Baskin, 2000).

Interaction between Cell Division and Cell Growth

For decades, cell biologists have been interested in the process that links cell size and cell division (Neufeld and Edgar, 1998), but the interaction is currently unclear. Some reports have argued that epidermal pavement cells of Arabidopsis leaves divide only rarely at a cell size larger than $400~\mu m^2$ (Donnelly et al., 1999; Geisler et al., 2000), suggesting a possible size threshold preventing cell division. By contrast, a study on the root meristem hinted at the lack of a maximum cell size threshold for cell division, because cells divide at very different sizes (Ivanov et al., 2002; Beemster et al., 2003). Similarly, our mathematical model suggests no threshold for cell division, because such a threshold would result in a deviation from the observed cell size distributions. Furthermore, cell size distributions show that the average pavement cell size increases during the proliferation phase. Thus, in the leaf epidermis, cells of different sizes divide, providing additional evidence for the nonexistence of a fixed threshold size for division. Moreover, the increase in cell size during proliferation points toward a disequilibrium between cell growth and cell division. The constant average cell cycle duration implies that this increase in cell size is due to relative cell expansion rates exceeding cell division rates, uncoupling cell size from cell division. In conclusion, in wild-type plants, cell division seems to be relatively independent of the status of cell expansion, whereas the cell cycle might act more as a timer than as a size-regulated machinery. Interestingly, studies of mutants and transgenic lines have revealed that cell division and cell expansion are somehow coordinated by multiple mechanisms, so that inhibition of one will be compensated by increased activity of the other and vice versa (Ferjani et al., 2007). The new model-based analysis of cell size distributions of mutants displaying this compensation phenomenon could be a manner to pinpoint the underlying mechanisms.

MATERIALS AND METHODS

Plant Material and Growth Conditions

Wild-type Arabidopsis (*Arabidopsis thaliana*) Heyhn. plants of the Columbia-0 accession were used for kinematic analysis of leaf growth. The plasma membrane marker 35S::GFP-PIP2a was used for live imaging of epidermal cell growth (Cutler et al., 2000). Seeds for in vitro analysis were sterilized in 3% bleach for 15 min and sown on medium containing 0.5× Murashige and Skoog medium (Duchefa) solidified with 9 g/L plant tissue culture agar (Lab M) on round plates (1013; Becton-Dickinson). After a stratification period of 2 d, the plates were placed in a growth chamber under long-day conditions (16 h of light, 8 h of darkness) at 22°C with a light intensity of 80 to 100 mE m^{-2} s^{-1} supplied by cool-white fluorescent tubes (Spectralux Plus 36W/840; Radium).

Kinematic Growth and Image Analysis

Leaf growth kinematics were analyzed as described (De Veylder et al., 2001). The leaf blade area of leaves 1 and 2 of five plants at 5 to 24 DAS was measured from dark-field binocular (days 8–24) or differential interference contrast light microscopy images (days 5–7). Microscopic drawings containing approximately 100 cells, located 25% and 75% from the tip and the base of the leaf blade on the abaxial side of each leaf were made with a drawing tube attached to the microscope equipped with differential interference contrast optics. The microscopic drawings were scanned for digitization. An in-house developed image analysis algorithm was subsequently used to automatically extract detailed measurements from the microscopic drawings, such as total area of the drawing, total number of cells, and number of stomata. Kinematic growth characteristics were calculated and plotted from these measurements. Extension of the image analysis algorithms allowed discrimination between pavement and guard cells and individual cell area measurements for these two cell types separately. Guard cells were extracted as cells <500 μm^2 neighboring the stomatal pores. The remaining cells were designated as pavement cells. These cell measurements were pooled by day and allowed the construction of cell area distributions. Therefore, cell areas of pavement and

guard cells were classified into bins of 100 μm^2 and 25 μm^2, respectively. Relative and absolute frequency distributions were plotted with MATLAB. The image analysis algorithms were written in C++ scripts and used the SDC morphology toolbox for C++ (www.mmorph.com/cppmorph/).

Live Imaging of Epidermal Cell Growth in the Leaf

At 16 DAS, three complete plants harboring the plasma membrane marker 35S::GFP-PIP2a (Cutler et al., 2000) were transferred under sterile conditions from in vitro plates to a round microscopic chamber (Warner instruments) with liquid 0.5× Murashige and Skoog growth medium (Duchefa). One leaf of the first leaf pair of each plant was flattened on the bottom of the chamber by overlaying it with a block of solidified agar. The abaxial epidermis was imaged with a confocal microscope with the software package LSM510 (Zeiss) from 17 to 18 DAS. Z stacks were recorded at five different positions with 12-h intervals over a total period of 36 h. Epidermal cells in the Z stacks were projected onto a single reconstructed view with the extended depth of field plug in (Forster et al., 2004) for ImageJ (http://rsbweb.nih.gov/ij). Cell lineages were manually tracked and measured at each time point with ImageJ. The RGRs for each cell were calculated as the average RGR of this cell over the different time intervals. Growth rates of 53 pavement cells and 13 guard cells were tracked over time.

Flow Cytometry Analysis

Plant material was chopped in 200 μL of Cystain UV Precise P Nuclei extraction buffer (Partec), supplemented with 800 μL of staining buffer. The mix was filtered through a 50-μm green filter and read through the Cyflow MB flow cytometer (Partec). The nuclei were analyzed with the FloMax software. The endoreduplication index was calculated from the percentages of each ploidy class with the formula: endoreduplication index = $(0 \times \%2C) + (1 \times \%4C) + (2 \times \%8C) + (3 \times \%16C) + (4 \times \%32C)$.

Supplemental Data

The following materials are available in the online version of this article.

Supplemental Figure S1. Experimental and smoothed total number of pavement and guard cells during leaf development.

Supplemental Figure S2. Validation of data extraction of two reference points for the whole-leaf cellular data analysis.

Supplemental Figure S3. Comparison between experimental and model-predicted cell size distributions of pavement cells.

Supplemental Figure S4. Comparison between experimental and model-predicted cell size distributions of guard cells.

Supplemental Figure S5. Result of 100 optimizations for the cell cycle duration.

Supplemental Figure S6. Putative recently divided pavement cells.

Supplemental Figure S7. Endoreduplication kinetics during leaf development.

Supplemental Table S1. Initial estimation of the average cell cycle duration T_c.

Supplemental Text S1. Mathematical description model.

LITERATURE CITED

Baskin TI (2000) On the constancy of cell division rate in the root meristem. Plant Mol Biol **43:** 545–554

Beemster GTS, Baskin TI (1998) Analysis of cell division and elongation underlying the developmental acceleration of root growth in *Arabidopsis thaliana.* Plant Physiol **116:** 1515–1526

Beemster GTS, De Veylder L, Vercruysse S, West G, Rombaut D, Van Hummelen P, Galichet A, Gruissem W, Inzé D, Vuylsteke M (2005) Genome-wide analysis of gene expression profiles associated with cell cycle transitions in growing organs of Arabidopsis. Plant Physiol **138:** 734–743

Beemster GTS, Fiorani F, Inzé D (2003) Cell cycle: the key to plant growth control? Trends Plant Sci **8:** 154–158

Benková E, Michniewicz M, Sauer M, Teichmann T, Seifertová D, Jürgens G, Friml J (2003) Local, efflux-dependent auxin gradients as a common module for plant organ formation. Cell **115:** 591–602

Bergmann DC, Sack FD (2007) Stomatal development. Annu Rev Plant Biol **58:** 163–181

Bowman JL (2000) Axial patterning in leaves and other lateral organs. Curr Opin Genet Dev **10:** 399–404

Campilho A, Garcia B, Toorn HV, Wijk HV, Campilho A, Scheres B (2006) Time-lapse analysis of stem-cell divisions in the *Arabidopsis thaliana* root meristem. Plant J **48:** 619–627

Cutler SR, Ehrhardt DW, Griffitts JS, Somerville CR (2000) Random GFP::cDNA fusions enable visualization of subcellular structures in cells of *Arabidopsis* at a high frequency. Proc Natl Acad Sci USA **97:** 3718–3723

de Almeida Engler J, De Veylder L, De Groodt R, Rombauts S, Boudolf V, De Meyer B, Hemerly A, Ferreira P, Beeckman T, Karimi M, et al (2009) Systematic analysis of cell-cycle gene expression during Arabidopsis development. Plant J **59:** 645–660

De Veylder L, Beeckman T, Beemster GTS, Krols L, Terras F, Landrieu I, Van Der Schueren E, Maes S, Naudts M, Inzé D (2001) Functional analysis of cyclin-dependent kinase inhibitors of *Arabidopsis*. Plant Cell **13:** 1653–1668

Donnelly PM, Bonetta D, Tsukaya H, Dengler RE, Dengler NG (1999) Cell cycling and cell enlargement in developing leaves of *Arabidopsis.* Dev Biol **215:** 407–419

Ferjani A, Horiguchi G, Yano S, Tsukaya H (2007) Analysis of leaf development in *fugu* mutants of Arabidopsis reveals three compensation modes that modulate cell expansion in determinate organs. Plant Physiol **144:** 988–999

Fernandez R, Das P, Mirabet V, Moscardi E, Traas J, Verdeil J-L, Malandain G, Godin C (2010) Imaging plant growth in 4D: robust tissue reconstruction and lineaging at cell resolution. Nat Methods **7:** 547–553

Fiorani F, Beemster GTS (2006) Quantitative analyses of cell division in plants. Plant Mol Biol **60:** 963–979

Forster B, Van De Ville D, Berent J, Sage D, Unser M (2004) Complex wavelets for extended depth-of-field: a new method for the fusion of multichannel microscopy images. Microsc Res Tech **65:** 33–42

Geisler M, Nadeau J, Sack FD (2000) Oriented asymmetric divisions that generate the stomatal spacing pattern in *Arabidopsis* are disrupted by the *too many mouths* mutation. Plant Cell **12:** 2075–2086

Green PB (1976) Growth and cell pattern formation on an axis: critique of concepts, terminology, and modes of study. Bot Gaz **137:** 187–202

Green PB, Bauer K (1977) Analysing the changing cell cycle. J Theor Biol **68:** 299–315

Hamant O, Heisler MG, Jönsson H, Krupinski P, Uyttewaal M, Bokov P, Corson F, Sahlin P, Boudaoud A, Meyerowitz EM, et al (2008) Developmental patterning by mechanical signals in *Arabidopsis*. Science **322:** 1650–1655

Ivanov VB, Dobrochaev AE, Baskin TI (2002) What the distribution of cell lengths in the root meristem does and does not reveal about cell division. J Plant Growth Regul **21:** 60–67

Keller CP, Van Volkenburgh E (1997) Auxin-induced epinasty of tobacco leaf tissues. Plant Physiol **113:** 603–610

Kotzer AM, Wasteneys GO (2006) Mechanisms behind the puzzle: microtubule-microfilament cross-talk in pavement cell formation. Can J Bot **84:** 594–603

Larkin JC, Marks MD, Nadeau J, Sack F (1997) Epidermal cell fate and patterning in leaves. Plant Cell **9:** 1109–1120

Liscum E, Stowe-Evans EL (2000) Phototropism: a "simple" physiological response modulated by multiple interacting photosensory-response pathways. Photochem Photobiol **72:** 273–282

Neufeld TP, Edgar BA (1998) Connections between growth and the cell cycle. Curr Opin Cell Biol **10:** 784–790

Panteris E, Galatis B (2005) The morphogenesis of lobed plant cells in the

mesophyll and epidermis: organization and distinct roles of cortical microtubules and actin filaments. New Phytol **167:** 721–732

Pien S, Wyrzykowska J, McQueen-Mason S, Smart C, Fleming A (2001) Local expression of expansin induces the entire process of leaf development and modifies leaf shape. Proc Natl Acad Sci USA **98:** 11812–11817

Reddy GV, Heisler MG, Ehrhardt DW, Meyerowitz EM (2004) Real-time lineage analysis reveals oriented cell divisions associated with morphogenesis at the shoot apex of *Arabidopsis thaliana.* Development **131:** 4225–4237

Reinhardt D, Mandel T, Kuhlemeier C (2000) Auxin regulates the initiation and radial position of plant lateral organs. Plant Cell **12:** 507–518

Roeder AHK, Chickarmane V, Cunha A, Obara B, Manjunath BS, Meyerowitz EM (2010) Variability in the control of cell division underlies sepal epidermal patterning in *Arabidopsis thaliana.* PLoS Biol **8:** e1000367

Savaldi-Goldstein S, Peto C, Chory J (2007) The epidermis both drives and restricts plant shoot growth. Nature **446:** 199–202

Sugimoto-Shirasu K, Roberts K (2003) "Big it up": endoreduplication and cell-size control in plants. Curr Opin Plant Biol **6:** 544–553

Swarup R, Kramer EM, Perry P, Knox K, Leyser HMO, Haseloff J, Beemster GTS, Bhalerao R, Bennett MJ (2005) Root gravitropism requires lateral root cap and epidermal cells for transport and response to a mobile auxin signal. Nat Cell Biol **7:** 1057–1065

Tsukaya H (2002) Interpretation of mutants in leaf morphology: genetic evidence for a compensatory system in leaf morphogenesis that provides a new link between cell and organismal theories. Int Rev Cytol **217:** 1–39

Ubeda-Tomás S, Federici F, Casimiro I, Beemster GTS, Bhalerao R, Swarup R, Doerner P, Haseloff J, Bennett MJ (2009) Gibberellin signaling in the endodermis controls *Arabidopsis* root meristem size. Curr Biol **19:** 1194–1199